Bifurcation and Stability Analysis of a One-Dimensional Diffusion-Autocatalytic Reaction System

B. De Dier, F. Walraven, R. Janssen, P. Van Rompay, and V. Hlavacek [1]

Dept. of Chemical Engineering, Katholieke Universiteit Leuven, Belgium, De Croylaan 2, B-3030 Leuven

Z. Naturforsch. **42 a,** 994–1004 (1987); received January 23, 1987

Results of a numerical analysis of a set of one-dimensional reaction-diffusion equations are presented. The basis of these equations is a model scheme of chemical reactions, involving auto- and cross-catalytic steps ("Brusselator"). The steady state problem is solved numerically, fully exploiting the properties of recently developed continuation codes. Bifurcation diagrams are constructed for zero flux boundary conditions. For a relatively large diffusivity of initial species the Brusselator displays a huge number of dissipative steady state structures. At low system lengths a mechanism of perturbed bifurcation may be percieved. Bifurcations coincide with turning points of asymmetric solution branches. Completely isolated solutions prove to exist as well. For the problem without limited diffusion of the initial species, a careful bifurcation analysis shows the existence of a number of higher order bifurcations. At some of these points asymmetric profiles emanate from other asymmetric structures. Bifurcation points and limit points do not necessarily coincide. Stability analysis shows that relatively few steady states are stable. Especially symmetric solutions are found to be stable.

1. Introduction

Since several decades, possible explanations for the genesis of spatial structures in living systems have found increasing interest. Lotka [1] proposed already seventy years ago that autocatalysis plays an important role in this spatial formation. Also Turing [2], studying a mathematical model of a growing embryo, agreed with this opinion. He suggested that a system consisting of chemical substances subject to reaction and transport, for example diffusion (but not by a hydrodynamic motion), should render possible the most important phenomena of morphogenesis. For such a system, the usual equilibrium state may become unstable under certain circumstances and become a non-uniform steady state. This idea of spatial structures developping through a sequence of "symmetry breaking" instabilities was proposed by Prigogine [3], and the resulting structures, occurring in reaction-diffusion systems, were called "dissipative structures". Prigogine demonstrated his ideas in a model which usually is referred to as the Brusselator.

Several authors have already investigated the Brusselator scheme. We refer to Nicolis [4], Herschkowitz-Kaufman [5, 6], Kubicek and Marek [7, 8, 9], and Hlavacek et al. [10–14]. Also other similar reaction schemes have been studied; for example an enzymatic reaction scheme [7], and a reaction scheme describing the metabolism of low molecular thiols and proteins [15].

In a previous paper [12] we studied the behaviour of the Brusselator scheme in one dimension for Dirichlet boundary conditions. The present paper reports on a study of this scheme for zero flux boundary conditions, the diffusion coefficient of the initial component A being infinite or limited. Three bifurcation diagrams will be depicted for these conditions. One of the main results is that the number of possible solutions decreases very quickly with decreasing diffusivity of component A. It also was observed that for the scaled $D_A = 0.5\ m^2$ a certain form of "composing of solutions" still exists.

2. Governing Equations

We consider the one-dimensional reaction-diffusion equations associated with the Brusselator

[1] Department of Chemical Engineering, S.U.N.Y. at Buffalo, Clifford C. Furnas Hall, Amherst 14260, New York USA.

Reprint requests to Prof. Van Rompay, Department of Chemical Engineering, Katholieke Universiteit Leuven, De Croylaan 2, B-3030 Leuven (Heverlee)/Belgien.

0932-0784 / 87 / 0900-0994 $ 01.30/0. – Please order a reprint rather than making your own copy.

model of Prigogine and Lefever [3]. The Brusselator corresponds to the reaction scheme:

$$A \xrightarrow{k_1} X\,,$$

$$B + X \xrightarrow{k_2} Y + D\,,$$

$$2X + Y \xrightarrow{k_3} 3X\,,$$

$$X \xrightarrow{k_4} E\,. \tag{1}$$

The rate equations for components A, B, X and Y are given by:

$$\frac{\partial \tilde{A}}{\partial \tilde{t}} = -k_1 \tilde{A} + \tilde{D}_A \frac{\partial^2 \tilde{A}}{\partial r^2}\,, \tag{2.1}$$

$$\frac{\partial \tilde{X}}{\partial \tilde{t}} = k_1 \tilde{A} - (k_2 \tilde{B} + k_4)\tilde{X} + k_3 \tilde{X}^2 \tilde{Y} + \tilde{D}_X \frac{\partial^2 \tilde{X}}{\partial r^2}\,, \tag{2.2}$$

$$\frac{\partial \tilde{Y}}{\partial \tilde{t}} = k_2 \tilde{B}\tilde{X} - k_3 \tilde{X}^2 \tilde{Y} + \tilde{D}_Y \frac{\partial^2 \tilde{Y}}{\partial r^2}\,, \tag{2.3}$$

$$\frac{\partial \tilde{B}}{\partial \tilde{t}} = -k_2 \tilde{B}\tilde{X} + \tilde{D}_B \frac{\partial^2 B}{\partial r^2}\,. \tag{2.4}$$

Here $\tilde{A}$, $\tilde{B}$, $\tilde{X}$ and $\tilde{Y}$ represent concentrations, D_A, D_B, D_X, D_Y are constant diffusion coefficients, r is the space coordinate and $\tilde{t}$ means time. Next the following scaled variables are introduced:

$$t = k_4 \tilde{t}, \qquad A = \left[\frac{k_1^2 k_3}{k_4^3}\right]^{1/2} \tilde{A}\,,$$

$$X = \left[\frac{k_3}{k_4}\right]^{1/2} \tilde{X}\,, \quad B = \left[\frac{k_2}{k_4}\right] \tilde{B}\,,$$

$$Y = \left[\frac{k_3}{k_4}\right]^{1/2} \tilde{Y}\,, \quad D_i = \frac{\tilde{D}_i}{k_4} \quad (i = A, B, X \text{ and } Y) \tag{3}$$

and $z = r/L$ where L is the reactor length.

After substitution of these scaled variables into the reaction equations (2), the following system of scaled equations is obtained:

$$\frac{\partial A}{\partial t} = -\frac{k_1}{k_4} A + \frac{D_A}{L^2} \frac{\partial^2 A}{\partial z^2}\,, \tag{4.1}$$

$$\frac{\partial X}{\partial t} = A - (B+1)X + X^2 Y + \frac{D_X}{L^2} \frac{\partial^2 X}{\partial z^2}\,, \tag{4.2}$$

$$\frac{\partial Y}{\partial t} = BX - X^2 Y + \frac{D_Y}{L^2} \frac{\partial^2 Y}{\partial z^2}\,, \tag{4.3}$$

$$\frac{\partial B}{\partial t} = -\left[\frac{k_2^2}{k_3 k_4}\right]^{1/2} BX + \frac{D_B}{L^2} \frac{\partial^2 B}{\partial z^2}\,. \tag{4.4}$$

Here A, B, X and Y are dimensionless concentrations, t is a dimensionless time, while the dimension of the diffusion coefficients becomes m^2; z is the dimensionless space coordinate and can take a value between 0 and 1. It has to be noted that due to this scaling quite realistic values of the diffusion coefficients correspond, in the scaled system (4), to numerical values of the coefficients of the order of unity. This point should be kept in mind in view of the computer simulations reported in this paper.

Two types of boundary conditions for X and Y may be considered.

Dirichlet boundary conditions are given by

$$t > 0\,; \quad z = 0, 1\,; \quad X = X_0\,, \quad Y = Y_0 \tag{5 a}$$

while zero flux boundary conditions are represented by

$$t > 0\,; \quad z = 0, 1\,; \quad (\partial X/\partial z) = 0\,, \quad (\partial Y/\partial z) = 0\,. \tag{5 b}$$

The boundary conditions for A and B are of the Dirichlet type since these are initial components.

$$t > 0\,; \quad z = 0, 1\,; \quad A = A_0\,, \quad B = B_0\,. \tag{5 c}$$

3. Numerical Solution Method

3.1. The Steady State Problem

The steady state equations can be derived from (4) by dropping the left hand side of these equations. We also assume that the rate constants k_i are equal to unity; then the next set of steady state equations is obtained.

$$\frac{d^2 A}{dz^2} = \frac{L^2}{D_A} A\,, \tag{6.1}$$

$$\frac{d^2 X}{dz^2} = \frac{L^2}{D_X}[(B+1)X - X^2 Y - A]\,, \tag{6.2}$$

$$\frac{d^2 Y}{dz^2} = \frac{L^2}{D_Y}[X^2 Y - BX]\,, \tag{6.3}$$

$$\frac{d^2 B}{dz^2} = \frac{L^2}{D_B} BX\,. \tag{6.4}$$

Together with the appropriate boundary conditions, these equations form a boundary value problem for ordinary differential equations. This problem was solved using a Stormer-Numerov difference approximation, thus obtaining a set of nonlinear algebraic equations which was solved using a Newton-Raphson technique. The Jacobian, used during the Newton-iterations, displays a band structure with bandwidth equal to 9. Taking advantage of this bandstructure, special linear system solvers from the NAG-library [16] were used.

Some, but not all of the reported solutions were checked by a method of shooting.

Complete solution branches were calculated by a continuation technique. For this purpose, first a straightforward continuation by varying the parameter L was used. Although such a strategy is economic in terms of computer time, it will not allow to solve the singular problems occurring at limit and bifurcation points. Therefore, in the vicinity of such points, specific continuation codes were invoked. For the bifurcation diagram reported in [17], the continuation algorithm applied was DERPAR [18]. However, full automation of DERPAR for more complicated problems was difficult to achieve. Therefore the results in this paper were based upon the PITCON-code developed by Rheinboldt and Burkardt [19]. This algorithm uses a local parametrization of the continuation problem, opposed to the code in [18] where an arc-length continuation is adopted. Furthermore, PITCON is able to detect bifurcation points of odd multiplicity. This feature, when fully exploited, is a great help in the construction of complete bifurcation diagrams.

4. Bifurcation Analysis

4.1. Zero Flux Boundary Conditions, Diffusivity of A Unlimited

In [20] a bifurcation analysis of the Brusselator is presented for the following set of parameters:

$$\begin{aligned} &D_A = \infty\,, \quad A_0 = 2.0\,,\\ &D_B = \infty\,, \quad B_0 = 4.6\,,\\ &D_X = 0.0016\ \mathrm{m}^2\,,\\ &D_Y = 0.0080\ \mathrm{m}^2\,. \end{aligned} \tag{7}$$

The distribution of the initial species A and B thus is homogeneous. For this system the following properties hold:

1. A trivial homogeneous solution exists regardless of the system length:
$$X = X_0 = A_0\,,$$
$$Y = Y_0 = B_0/A_0\,.$$
2. By perturbation analysis two elementary primary bifurcation lengths $L_{1,2}$ may be calculated:
$$L_{1,2} = n\pi\left[\frac{1}{2D_X}\left[B - 1 - \frac{A^2}{\Omega} \pm \sqrt{\left[1 - B + \frac{A^2}{\Omega}\right]^2 - \frac{4A^2}{\Omega}}\right]\right]^{-1/2}.$$
Here Ω represents D_Y/D_X.

   With the set of parameters reported above one can verify that $L_1 = 0.0798$ and $L_2 = 0.2212$ (arbitrary space units).
3. The primary bifurcation at $L_{1,2}$ yields elementary closed loops of steady state solutions.
4. By the possibility of composing elementary solutions, see [6], an elaborated bifurcation diagram may be constructed.
5. Secondary bifurcation occurs at points where primary solutions with different wavenumber coincide.

The bifurcation pattern may be derived from the following considerations, see Figure 1:

1. At the primary bifurcation point PB1 two half-rays of asymmetric solutions emanate. The profiles of X and Y on these half-rays are mirror-reflections of each other.
2. The point PB1 may be seen as the place where these reflections coincide in a symmetric (trivial) state.
3. The two half-rays evolve in the bifurcation diagram under the constraint of mirror symmetry. At the place where they meet again two asymmetric solutions coincide with a symmetric solution. Apparently this is at the point SB. Since SB is not the trivial state, this bifurcation is termed secondary. Actually the curve through SB is a primary branch starting at PB2 where the reactorlength L equals $2L_1$.

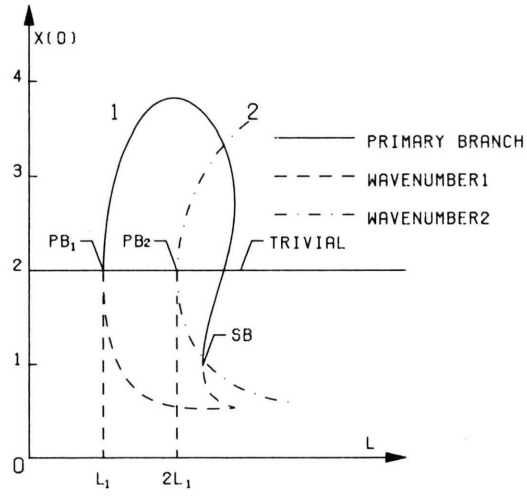

Fig. 1. Construction of the bifurcation diagram.

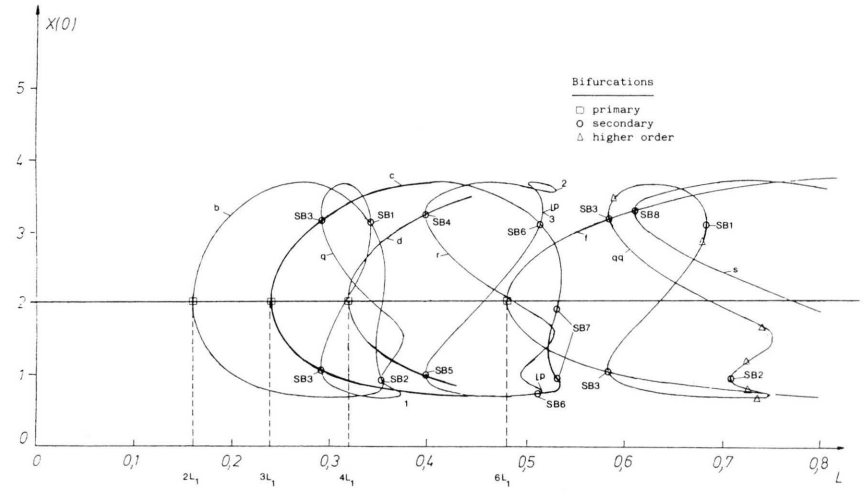

Fig. 2. Part of the bifurcation diagram for infinite diffusivity of component *A*.

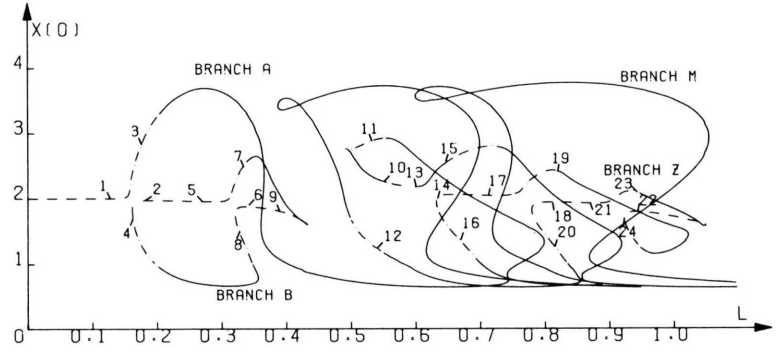

Fig. 7. Evolution of symmetric branches for $D_A = 0.5\,\mathrm{m}^2$.

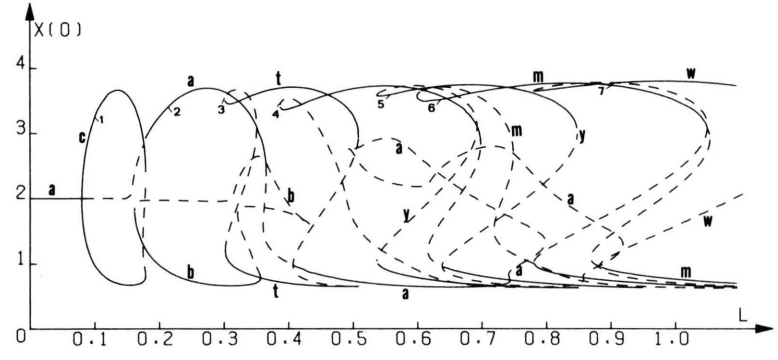

Fig. 10. Stability analysis of the bifurcation diagram for $D_A = 0.5\,\mathrm{m}^2$.

4. From symmetry considerations it follows that PB1 and SB at the same time must be limit points of the asymmetric solution curve 1.

A careful numerical investigation, however, did demonstrate the existence of yet other solutions, having characteristics differing deeply from already reported ones:

1. The solution branches contain only bifurcation points of higher than primary order.
2. The nature of the bifurcation may be asymmetric → asymmetric.
3. It is possible that bifurcation points do not coincide with limit points of asymmetric solution curves.

Following the dependence on the length L of one of the curves q, qq or r in Fig. 2, the aforementioned statements may be verified.

Figure 2 partly depicts results from [20], i. e. the primary branches b, c, d and f, bifurcating at $2L_1$, $3L_1$, $4L_1$ and $6L_1$ respectively, where L_1 denotes the first of the elementary lengths $L_{1,2}$ (see p. 997).

The curves q, qq and r were not reported in [20]. The bifurcation pattern for curve r is as follows:

1. At SB4 two half-rays of asymmetric solutions arise from curve d. The latter one is a locus of symmetric solutions since it bifurcates at an even multiple of L_1.
2. The two half-rays evolve in the diagram until at SB6 two mirror-symmetric profiles of branch r coincide with two mirror-symmetric profiles on c, which is a primary branch bifurcating at $3L_1$.
3. At the bifurcation point the profiles on c and on r are the same. The locus of intersection, however, is not a single point. The bifurcation place is a set of two split points SB6 in the diagram.
4. The points SB6 do not fall in the limit point of either curve c or r. In Fig. 2 the limit points closest to SB6 are designated LP. SB6 and LP are clearly distinct states. Symmetry considerations imply that the non-coincidence of limit points and bifurcation points is entirely due to the type of bifurcation. Opposed to SB4, the nature of the bifurcation at SB6 is asymmetric → asymmetric.
5. From the points SB6 the two half-rays of solutions proceed until at SB5 they meet again. SB5 is a bifurcation point of the class of SB4.

The same reasoning applies for branch q. The involved bifurcation points are SB1, SB3 and SB2, in order.

The possibility of composing solutions also holds for branches picturing only secondary bifurcations; for instance, branch qq may be derived entirely from branch q by simple translation and appropriate expansion. In this way, profiles for particular values of L on qq correspond to twofold concatenation of solutions on q at $L/2$. Bifurcation points on qq are termed SB1, SB2 and SB3, see Figure 2.

Branches q and r are members of a new class of elementary solutions that may be added to the already known primary branches in [20]. This new class is characterized by bifurcations of higher than primary order. Bifurcation happens at a symmetric branch. A closed loop results which returns to the same branch. Branches q and r are only representatives of this new class. Indeed, e. g. on branch c (Fig. 2) another split bifurcation point SB7 is indicated. SB7 has the same nature as SB3 and SB6. Also on branch f, the primary branch bifurcating at $6L_1$, a bifurcation SB8 (see Fig. 2) was found which has no analogue on branch c bifurcating at $3L_1$. Part of the bifurcating branch s is depicted in Figure 2.

The conclusion is that the number of possible states due to secondary bifurcation strongly increases with the dimension of the system. Moreover, with increasing length L, bifurcations of still higher

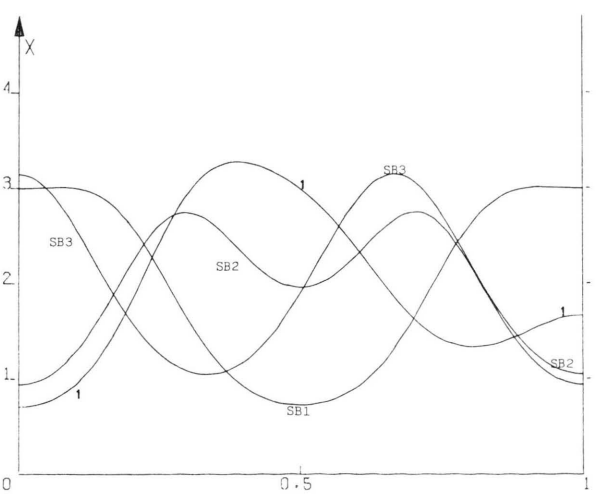

Fig. 3. Concentration profiles for selected points on branch q.

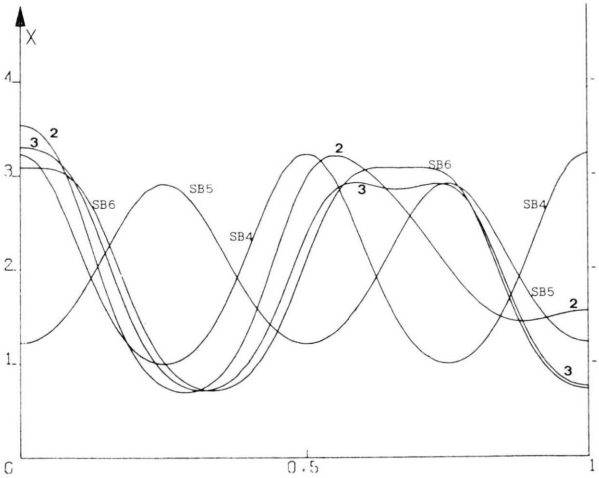

Fig. 4. Concentration profiles for selected points on branch r.

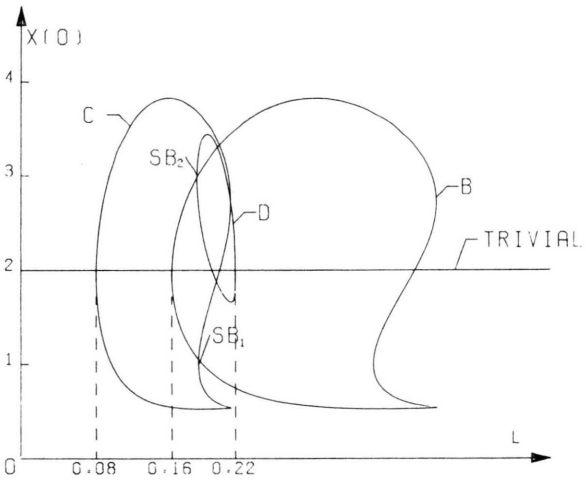

Fig. 5. Location of the bifurcation points on the diagram for infinite D_A.

order are possible. For instance on the secondary branch qq a number of tertiary bifurcations may occur, see Figure 2. The analogues of these points cannot be located on the elementary branch q. Taking into account these considerations, it follows that the explicit formula in [20] for the total number of solutions only applies to primary states.

Indication of bifurcation points was obtained through extensive use of PITCON for continuation. Particular profiles for component X on the secondary branches q and r are drawn in Figs. 3 and 4. Numbers in Fig. 2 and Figs. 3 and 4 correspond. We remark that for any asymmetric solution the mirror-symmetry is a solution as well. However, they have not been drawn in order not to overload the picture. Relevant profiles for Y may be found in [14]. For primary states we refer to [20].

4.2. Zero Flux Boundary Conditions, Limited Diffusivity of A

Since the diffusion of component A is limited, its distribution is no longer homogeneous. From (6.1) it can be computed [12] that in this case the profile of A corresponds to

$$A(z) = A_0 \frac{\cosh(2\alpha L(z-0.5))}{\cosh(\alpha L)},$$

where $\alpha = (4 D_A)^{-0.5}$.

(i) Region of Larger Diffusivity of A

The relevant set of parameters is taken as

$$D_A = 0.5 \text{ m}^2, \quad A_0 = 2.0,$$
$$D_B = \infty, \quad B_0 = 4.6,$$
$$D_X = 0.0016 \text{ m}^2,$$
$$D_Y = 0.0080 \text{ m}^2.$$

Just as for Dirichlet boundary conditions [17] a perturbed bifurcation mechanism is observed, involving the trivial homogeneous solution and the first bifurcating symmetric solution for $D_A = \infty$. For zero flux boundary conditions the latter solution emanates at $2L_1$. Partial results for $D_A = \infty$ and zero flux boundary conditions are summarized in Figure 5.

This figure depicts the first primary bifurcations from the trivial state. Curves c and d emanating at $L_1 = 0.08$ and $L_2 = 0.22$ (arbitrary space units), respectively, are branches of asymmetric elementary solutions. Curve b is the first bifurcating loop of symmetric states. Points SB1 and SB2 in Fig. 5 depict secondary bifurcations where two asymmetric states collapse in a symmetric one.

The analogue situation for $D_A = 0.5 \text{ m}^2$ is given in Figure 6:

1. The trivial solution in Fig. 5 is replaced by a branch of states exhibiting spatial dependence. This branch in Fig. 6 will be termed as basic state (A).

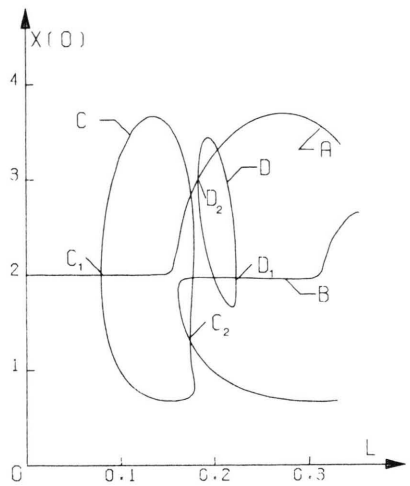

Fig. 6. Location of the bifurcation points on the diagram for $D_A = 0.5\,\mathrm{m}^2$.

2. From comparison of Figs. 5 and 6 it follows that for a reactorlength $L \leqq 0.16$ m, i.e. $L \leqq 2L_1$, the basic branch A (Fig. 6) nearly coincides with the homogeneous trivial state (Figure 5).
3. The primary bifurcation of symmetric state B (Fig. 5) vanishes. Instead, the involved branch decomposes due to a perturbed bifurcation:

   a) Structures with $X(0) > 2.0$ for $D_A = 0.5\,\mathrm{m}^2$ move to the basic state A (Figure 5). Indeed, for $0.16\,\mathrm{m} < L < 0.30\,\mathrm{m}$, the basic branch follows closely the dependence of branch B of symmetric states in Figure 5. Of course, this almost coincidence not only applies to $X(0)$ but to the whole dependence $X(z)$, $Y(z)$ for $z = 0.1$.

   b) Structures with $X(0) < 2.0$ for $D_A = 0.5\,\mathrm{m}^2$ stay on the lower part of branch B (Figure 5).
4. In Fig. 5 for $D_A = \infty$, the curve C of elementary solutions appears through a primary bifurcation at $L = L_1 = 0.08$ m. The secondary bifurcation point SB1 is common between curves C and B. The situation for $D_A = 0.5\,\mathrm{m}^2$ is almost unaltered. Curve C of asymmetric solutions again emanates from the basic state at $L = 0.08$ m (Fig. 6, point C1). The bifurcation point C2 in Fig. 6 depicts solutions common to branches C and B.
5. In Fig. 5 the elementary curve D is yielded through primary bifurcation at $L_2 = 0.22$ m. At the secondary bifurcation point SB2, solutions on curves D and B coincide. In Fig. 6 the location of the latter point is nearly unaffected (point D2). However, primary bifurcation from the trivial state shifts into bifurcation from curve B near $L = 0.22$ m. From this point of view, the trivial behaviour for $D_A = 0.5\,\mathrm{m}^2$ and $0.16\,\mathrm{m} < L < 0.30\,\mathrm{m}$ is mediated by the upper part of branch B. Moreover, near $L = 0.31$ m this part of branch B moves into the region $X(0) > 2.0$. Hereby identical structures are built which for $D_A = \infty$ appear through primary bifurcation at $L = 4L_1 = 0.32$ m.

The complete bifurcation diagram for zero flux boundary conditions and $D_A = 0.5\,\mathrm{m}^2$ comprises a very large number of different solution branches. It may be found in [11]. The total number of different solution branches reported for $0.0\,\mathrm{m} < L < 1.1\,\mathrm{m}$ is 23. Four of these branches consist of symmetric dissipative structures. The diagram was constructed taking full advantage of the bifurcation detection property of the PITCON-routine.

The evolution of the symmetric curves is displayed more clearly in Figure 7 (see p. 997):

1. Curve A: For low reactorlength L this branch corresponds to the thermodynamic state. For $L < 1.1$ m the number of bifurcation points on this basis is 26. The number of turning points for branch A on Fig. 7 is 12.
2. Curve B is a closed loop of symmetric solutions triggered by a perturbed bifurcation mechanism.
3. Curve Z is a closed loop of symmetric solutions.
4. Curve M: On Fig. 7 curve M is open. However it may close at a length larger than 1.1. Another possibility is that M is just another part of the basic branch A, which at higher length may return after a turning point.

A relation may be drawn between the bifurcation diagrams for $D_A = \infty$ and $D_A = 0.5\,\mathrm{m}^2$. Therefore we compare the symmetric states in the vicinity of $L = 2L_1$, $4L_1$, $6L_1$, $8L_1$, $10L_1$ and $12L_1$, i.e. $L = 0.16$ m, 0.32 m, 0.48 m, 0.64 m, 0.80 m and 0.96 m, respectively. We recall that at these lengths for $D_A = \infty$ symmetric solutions bifurcate characterized by wavenumbers 2, 4, 6, 8, 10 and 12. These structures are 2-fold, 4-fold, 6-fold ... concatenations of elementary asymmetric solutions. The exact

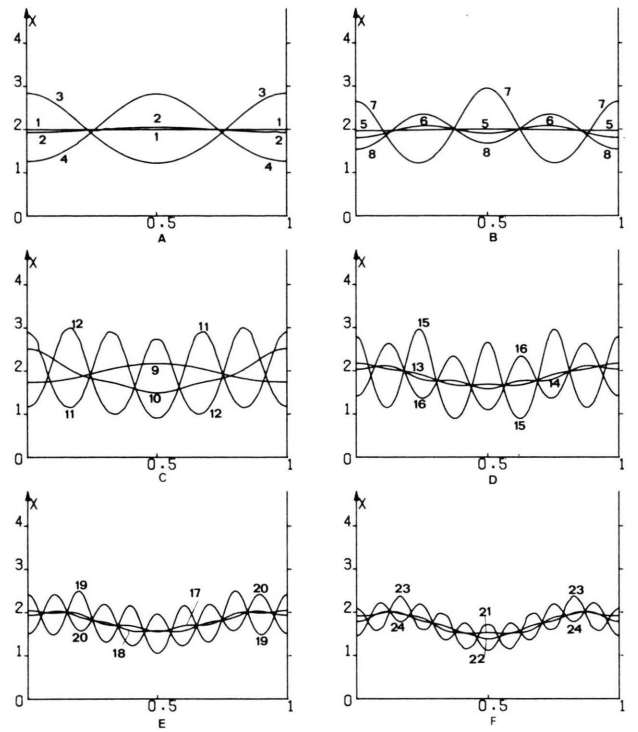

Fig. 8. Concentration profiles for selected points of the bifurcation diagram for $D_A = 0.5\,\mathrm{m}^2$.

composition of the solution for $D_A = 0.5\,\mathrm{m}^2$ can no longer be valid, as a consequence of the spatial dependence of A. However, in the vicinity of aforementioned lengths symmetric structures with a "correct" wavenumber still exist. These structures always appear in pairs which do not necessarily lie on the same branch. One element of this pair has $X(0) > 2.0$ and $Y(0) < 2.3$, while the other has $X(0) < 2.0$ and $Y(0) > 2.3$. Moreover, at the places in the bifurcation diagram where these structures occur, anytime another part of a symmetric curve may be localized where the spatial distribution of X and Y approaches homogeneity. In this respect these portions of curves interpret the role of the former trivial solution.

The situation is visualized in Figs. 7 and 8. In Fig. 7 parts of curves where solutions display a certain wavenumber are drawn as dash dotted lines, portions of curves approximating homogeneous distribution of X and Y are drawn as dashed line. Corresponding spatial profiles for X are given in Figure 8.

The number of asymmetric branches is 19. Four of these branches are involved in a bifurcation pattern symmetric → asymmetric → symmetric → asymmetric → symmetric, yielding two different families of solutions. One of these subsets has already been displayed in Figure 6. It involves the symmetric branches A and B and the asymmetric branches C and D.

Fourteen asymmetric solution curves have their two bifurcation points on the same symmetric branch, seven of them bifurcate on the basic branch, two on branch B, three on branch Z and two on branch M.

Just as for Dirichlet boundary conditions [17] one asymmetric branch is fully isolated. No bifurcation points could be found on it. This branch displays itself in the bifurcation diagram as two split loops, each depicting the boundary value of X at one end of the reactor. Diagrams of all the solution branches described, may be found in [11] together with the spatial profiles for the intermediates X and Y.

(ii) Region of Smaller Diffusivity of A

Figure 9 is the bifurcation diagram for $D_A = 0.02\,\mathrm{m}^2$ [14]. All other parameters are as in set (7). Part of the results for $D_A = 0.5\,\mathrm{m}^2$ also apply for $D_A = 0.02\,\mathrm{m}^2$, i. e.:

1. The first bifurcating symmetric solution is involved in a perturbed bifurcation mechanism.
2. Two symmetric and two asymmetric branches are chained in a pattern of bifurcation symmetric → asymmetric. This subset of solutions concerns the branching in Table 1.

Table 1. Solution set for $D_A = 0.02\,\mathrm{m}^2$, zero flux B.C.

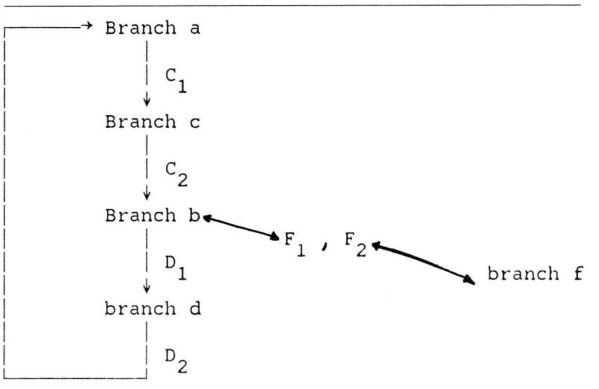

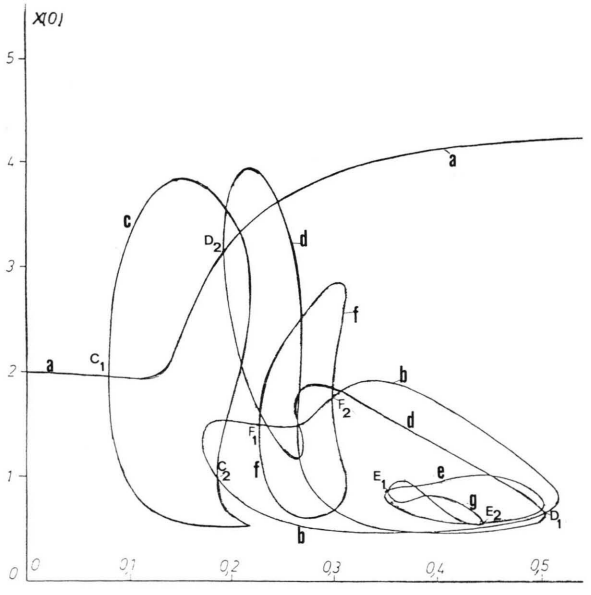

Fig. 9. Bifurcation diagram for $D_A = 0.02\ m^2$.

The location of the points C1, C2 and D2 for $D_A = 0.5\ m^2$ and $D_A = 0.02\ m^2$ correspond fairly well. However, for $D_A = 0.02\ m^2$ point D1 moves to a much higher length and to qualitatively different spatial distributions for X and Y.

3. As indicated in Table 1, the asymmetry f has two bifurcation points on branch b.
4. No other bifurcations than symmetric → asymmetric have been percieved.

The diagram for $D_A = 0.02\ m^2$ contains a totally isolated loop (branch e in Figure 9). In contrast to earlier results this loop is a branch of symmetric solutions. It has two more bifurcation points giving rise to curve g.

By comparison of the results for $D_A = 0.5\ m^2$ and $D_A = 0.02\ m^2$, and since the concentration of component A decreases for a smaller D_A [10], it follows that for small values of the diffusitivity D_A:

1. The course of the basic branch a is much simpler and doesn't lead to a variety of spatial patterns, cf. Figs. 7 and 9, since essentially bifurcations of this state give rise to a multitude of solutions.
2. The number of dissipative structures is strongly reduced. The same conclusion applies for Dirichlet boundary conditions [11].

5. Stability Analysis

5.1 The Transient Equations

The set of coupled partial differential equations (4) was solved using a Crank-Nicholson technique with self adjusting timestep. Details of this procedure may be found in [6]. The solutions of the steady state equations were slightly perturbed and served as initial conditions for the numerical integration of the set (4). In contrast to [6], where distortions of the time-independent solutions were applied locally in a limited number of grid points, in this work the steady state as a whole was perturbed. It is known that a Crank-Nicholson technique, which is a combination of an implicit and an explicit scheme, should not be affected by the value of the timestep taken. For this work an initial timestep between 0.001 and 0.0001 was used; according to the convergence rate of a previous profile the timestep could then be enlarged or decreased for the calculation of the next profile.

5.2 Zero Flux Boundary Conditions

(i) Region of Larger Diffusivity of A

The diagram for $D_A = 0.5\ m^2$ described earlier was subject to stability calculations [11]. The results are shown in Figure 10. For the sake of clarity, only branches displaying stable parts are depicted. Full lines correspond to stable solutions, dashed lines to unstable profiles. From Fig. 10 it may be inferred that switching of stability occurs at bifurcation and limit points (see p. 997).

A number of conclusions can be drawn, some of which also apply for Dirichlet boundary conditions.

1. Compared to the total number of stationary patterns, only a few steady states are stable. Their existence is limited to the basic branch a and to the branches b, m, c, t, y and w.
2. Especially symmetric branches are found to be stable. However, no stable parts could be detected on the symmetric branch z (see Figure 7).
3. The major part of asymmetric solutions reported in the first part of this paper (see also [11]) prove to be unstable. In contrast to Dirichlet boundary conditions, $D_A = 0.1\ m^2$, where for all lengths

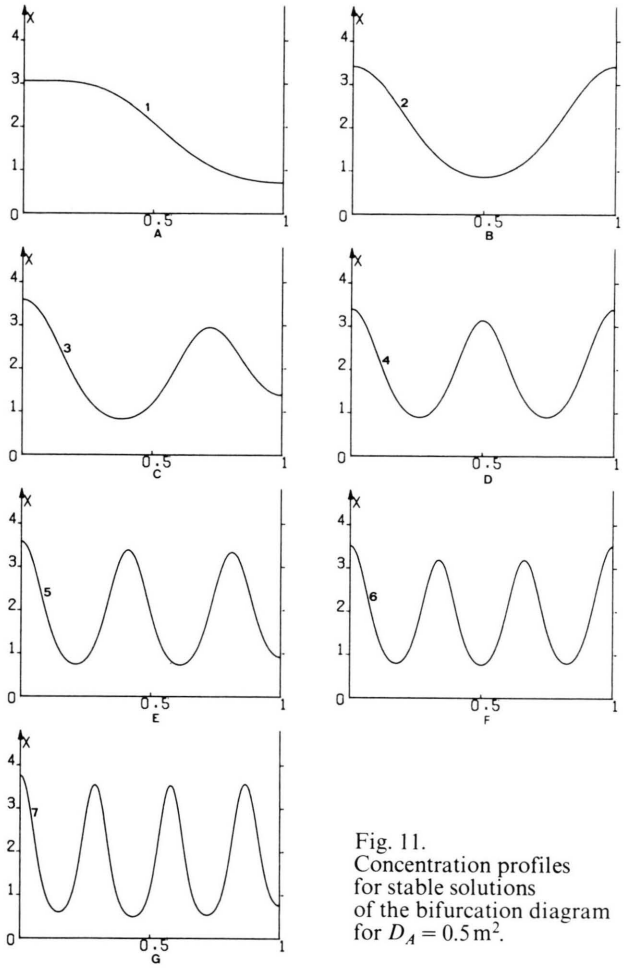

Fig. 11.
Concentration profiles
for stable solutions
of the bifurcation diagram
for $D_A = 0.5\,\mathrm{m}^2$.

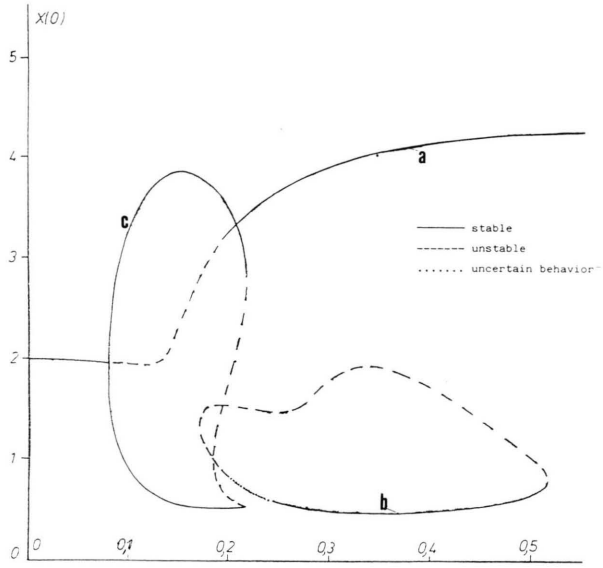

Fig. 12. Stability analysis of the bifurcation diagram for $D_A = 0.02\ \mathrm{m}^2$.

L at least one symmetric solution was stable, the diagram in Fig. 10 depicts some intervals for L where stability only occurs on asymmetric structures, e.g. $0.1\ \mathrm{m} < L < 0.15\ \mathrm{m}$. In the same way some ranges of L only have symmetric stable solutions, e.g. $0.2\ \mathrm{m} < L < 0.3\ \mathrm{m}$.

4. According to Fig. 10 the maximum number of stable patterns for some length L is 6. Where this number is greater than 2, always two mirror-symmetric asymmetries are involved.
5. Just as for Dirichlet boundary conditions and large D_A, stable steady states concentrate on the outside of the diagram. Such profiles are characterized by a strong spatial dependence of X and Y. None of the small amplitude symmetric solutions on branches a, b, z or m prove to be stable.
6. With growing length L the number of modes on stable branches steadily increases. Thus, stable profiles for higher L depict a more and more pronounced spatial dependence. This is illustrated in Fig. 11, where X-profiles for subsequent stable solutions are displayed. Numbers in Figs. 10 and 11 correspond.

(ii) Region of Smaller Diffusivity of A

The stability diagram for $D_A = 0.02\ \mathrm{m}^2$ [14] is shown in Figure 12. Again only branches with stable parts are depicted.

Occurrence of stable solutions is limited to the basic branch a, the asymmetric branch c and the symmetric branch b. No parts of branches d, f, e and g, see Fig. 9, was found to be stable.

Again stable profiles are high amplitude solutions, exception made of course for the close to trivial structure on the basic branch ($0 < L < 0.08$ m).

[1] A. J. Lotka, J. Phys. Chem. **14,** 271 (1910).
[2] A. M. Turing, Phil. Trans. Roy. Soc.London **B237,** 37 (1952).
[3] I. Prigogine and R. Lefever, J. Chem. Phys. **48,** 1695 (1968).
[4] G. Nicolis and I. Prigogine, Self Organization in Non-Equilibrium Systems, John Wiley, New York 1977.
[5] M. Herschkowitz-Kaufman and G. Nicolis, J. Chem. Phys. **56,** 1890 (1972).
[6] M. Herschkowitz-Kaufman, Bull. Math. Biol. **37,** 589 (1975).
[7] M. Kubicek and M. Marek, J. Chem. Phys. **67,** 1997 (1977).
[8] M. Kubicek, V. Ryzler, and M. Marek, Biophys. Chem. **8,** 235 (1978).
[9] M. Marek and M. Kubicek, Z. Naturforsch. **35 a,** 336 (1980).
[10] R. Janssen, Ph.D. Thesis, Katholieke Universiteit Leuven, Faculty of Applied Sciences, 1984.
[11] B. De Dier, Eng. Thesis, Katholieke Universiteit Leuven, Faculty of Applied Sciences, 1984
[12] V. Hlavacek, R. Janssen, and P. Van Rompay, Z. Naturforsch. **37 a,** 39 (1982).
[13] P. Nandapurkar and V. Hlavacek, Z. Naturforsch. **38 a,** 963 (1983).
[14] F. Walraven, Eng. Thesis, Katholieke Universiteit Leuven, Faculty of Applied Sciences, 1983.
[15] M. Kubicek, M. Marek, P. Hustak, and V. Ryzler, Proc. of the 5-th Symposium on "Computers in Chemical Engineering", 5–9 oct. 1977, High Tatras, Czechoslovakia, p. 903–939.
[16] Nag Manual, Mark 8, Numerical Algorithms Group, Oxford 1980.
[17] R. Janssen, V. Hlavacek, and P. Van Rompay, Z. Naturforsch. **38 a,** 487 (1983).
[18] M. Kubicek, Acm Trans. Math. Softw. **2,** 98 (1976).
[19] W. C. Rheinboldt and J. V. Burkhardt, Acm Trans. Math. Softw. **9,** 215 (1983).
[20] M. Kubicek, V. Ryzler, and M. Marek, Sci. Papers Prague Instit. of Chemical Technol. **K 14,** 147 (1979).